Identification of lifetime limiting defects by temperature- and injection-dependent photoluminescence imaging

Jonas Schön,[1] Amanda Youssef,[2] Sungeun Park,[3] Laura E. Mundt,[1] Tim Niewelt,[1] Sebastian Mack,[1] Kazuo Nakajima,[4] Kohei Morishita,[5] Ryota Murai,[4] Mallory A. Jensen,[2] Tonio Buonassisi,[2] and Martin C. Schubert[1]

[1]*Fraunhofer Institute for Solar Energy Systems, Heidenhofstraße 2, D-79110 Freiburg, Germany*
[2]*Massachusetts Institute of Technology, Cambridge, Massachusetts 02139, USA*
[3]*Department of Materials Science and Engineering, Korea University, 145 Anam-ro, Seongbuk-gu, Seoul 136-713, South Korea*
[4]*FUTURE-PV Innovation, Koriyama, Fukushima 963-0215, Japan*
[5]*Kyoto University, Yoshida-Honmachi, Sakyo-Ku, Kyoto 606-8501, Japan*

(Received 21 June 2016; accepted 9 August 2016; published online 8 September 2016)

Identification of the lifetime limiting defects in silicon plays a key role in systematically optimizing the efficiency potential of material for solar cells. We present a technique based on temperature and injection dependent photoluminescence imaging to determine the energy levels and capture cross section ratios of Shockley–Read–Hall defects. This allows us to identify homogeneously and inhomogeneously distributed defects limiting the charge carrier lifetime in any silicon wafer. The technique is demonstrated on an n-type wafer grown with the non-contact crucible (NOC) method and an industrial Czochralski (Cz) wafer prone to defect formation during high temperature processing. We find that the energy levels for the circular distributed defects in the Cz wafer are in good agreement with literature data for homogeneously grown oxide precipitates. In contrast, the circular distributed defects found in NOC Si have significantly deeper trap levels, despite their similar appearance. *Published by AIP Publishing*. [http://dx.doi.org/10.1063/1.4961465]

I. INTRODUCTION

Besides the most prominent defects in p-type silicon, i.e., the boron oxygen (BO) defect in Czochralski (Cz) silicon and interstitial iron in multicrystalline (mc) silicon, little is known about the relevance of the various limiting defects in different silicon materials. However, the identification of the lifetime limiting defects allows to systematically exploiting the efficiency potential of the material. Despite their significant impact on solar cell performance the concentrations of these defects are usually very small and thus are best detected with lifetime measurements. The metastability of BO defects, interstitial Fe and Cr in p-type silicon can be used to quantify their impact on the charge carrier lifetime by photoluminescence (PL) imaging in their two metastable states.[1–4] However, this approach cannot be applied to Fe_i and Cr_i in n-type silicon or other defects without metastability. The defect parameters, i.e., the energy level and the capture cross-sections for holes and electrons, are known for a variety of defects (see, e.g., Ref. 5 for an overview) from deep-level transient spectroscopy (DLTS) or injection- and temperature-dependent lifetime measurements[6–8] applied to intentionally contaminated samples.

Temperature- and injection-dependent photoluminescence imaging (TIDPLI) can be used to identify the dominant defects and their concentrations for lifetime limitation of two or three defects. We have demonstrated earlier that this TIDPLI technique yields similar concentrations of Fe_i and Cr_i as measured by the metastable technique.[9]

In this work, the technique is further improved and applied to circular distributed defects in n-type Cz and non-contact crucible (NOC) silicon. In contrast to the injection-dependent lifetime spectroscopy,[6,7] the proposed technique aims to identify the dominant defects in a given sample and not to precisely determine the energy level and the capture cross section ratio in intentionally contaminated samples with different doping concentration. The drawback of this significant simplification is a higher inaccuracy of the calculated defect parameters. The use of an imaging technique also allows for the determination of the defect parameters at every pixel and therefore the characterization of laterally inhomogeneously distributed defects.

Circular defect patterns have been observed in Cz silicon wafers after high temperature processing, such as thermal oxidation.[10] It is assumed that these defects are oxide precipitates[10,11] decorated with metal impurities.[7] Before the high temperature process, the oxide precipitates are small and unstrained and thus have a negligible impact on the minority charge carrier lifetime. However, as they grow larger, e.g., by thermal processing, they punch-out crystallographic defects[11] and become decorated with metal impurities.[12] The presence (or absence) of the defects depends on the oxygen concentration, the thermal history, and the concentration of vacancies which are believed to influence the ring-like structure.[10] These defects are detrimental to the minority charge carrier lifetime and thus can lead to significant reduction in conversion efficiency.[10,13]

In Si wafers grown by the non-contact crucible (NOC) method,[14] which have a comparable oxygen concentration as wafers fabricated by the Cz method, a similar circular pattern was observed after high temperature processing.[15] NOC is an emerging growth technique, intended to minimize cost compared with Cz by increasing throughput and minimize

impurity content compared with mc Si by avoiding contact between the solidified ingot and the crucible.[16]

From an extensive study of intentionally grown oxide precipitates in n-and p-type silicon Murphy *et al.*[7,17] determined the defect parameters of oxide precipitates in Cz Si and concluded that oxide precipitates can be described by two independent Shockley–Read–Hall (SRH) defects. The injection- and temperature-dependent lifetime analysis presented in this work allows us to determine whether the laterally inhomogeneous defect occurrence in the analyzed industrial n-type Cz Si and NOC Si can also be described with these two SRH defects and are thus all the same defects.

II. SAMPLES, PREPARATION, AND MEASUREMENTS

The studied n-type six-inch Cz-Si wafers feature a resistivity of 2.8 Ω cm and a final thickness of 140 μm. The NOC samples originate from one 180 μm wafer from the top of the ingot, which is cut to pieces 4 cm × 5 cm large equidistant to the center. We study three Cz and NOC Si wafers: (1) one is left in the as-grown state, (2) one is subjected to phosphorus diffusion gettering at 860 °C, and (3) one is subjected to the same phosphorus diffusion followed by thermal oxidation at 1000 °C. After removal of both the thermal oxide layer and diffused region, all samples are passivated with a silicon nitride layer deposited by plasma-enhanced chemical vapor deposition (PECVD) at 250 °C on both sides.

The photoluminescence intensities under varied injection conditions are measured for temperatures between 25 °C and 160 °C (200 °C for Cz Si samples) using a 1 megapixel CCD luminescence imaging setup. The PL images are calibrated to lifetime images with a self-consistent modulated PL measurement[18] at the corresponding temperature. We are able to cover a wide injection range in our PL measurements via variation of the 790 nm laser illumination intensity between 0.0002 and more than 10 sun equivalents. The charge carrier lifetime in the edge regions of the n-type Cz Si wafers increases with the phosphorus diffusion, whereas in the center it drops significantly after additional oxidation and low lifetime rings become visible in the measurements at 25 °C (see Figures 1(a) and 1(b)). The injection-dependent lifetimes of the oxidized sample, averaged in the defect region marked with a green rectangle in Figure 1(b), are shown in Figure 2(a) for temperatures from 25 °C to 160 °C. Following the notation of Murphy *et al.*[7] the lifetime of n-type samples is plotted over the ratio to holes and electrons $Y = p/n \approx \Delta n/(n_0 + \Delta n)$, with the excess carrier concentration Δn and the doping concentration n_0. In this notation, the lifetime of a single SRH defect is linear which simplifies the analysis.

Despite correcting for the Auger recombination influence,[19] the injection-dependent lifetime at 25 °C has an increasing and a decreasing injection regime, as apparent from Figure 2(a). This indicates the necessity of assuming two SRH defects to describe the lifetimes measured at the circular low lifetime region. SRH lifetimes in both the low and the high injection regimes increase with temperature in the circular low lifetime region. As a result, the contrast in the images related to the circular distributed defects becomes less pronounced with increasing temperature and the rings vanish completely at 200 °C in the whole injection regime (see Figure 1(d)). The significant change in the injection dependent lifetime is a first indication that the energy levels of the defects are not in the middle of the bandgap.[7]

The NOC samples are even more affected by the oxidation than the Cz samples (Figures 1(e) and 1(f)). The lifetime drops by more than one order of magnitude after oxidation. Besides the very low lifetime rings, a microstructure appears. The average injection-dependent lifetime in the center part is shown for different temperatures in Figure 2(b). Despite laser intensities of around 8 sun equivalents, the charge carrier ratio Y is below $Y = 0.4$ due to the low lifetime of the sample. As a consequence, we are less sensitive to shallow defects, which become more important at high injection levels. In contrast to the lifetime of the lower doped Cz Si sample (that decreases for $Y > 0.2$) the lifetime of the NOC Si sample increases in the whole measured injection regime. Thus, we can exclude a strong lifetime limitation of the defect found in the Cz Si sample which caused a decreasing lifetime at high injection although we are not able to reach Y above 0.5 in the NOC Si sample. Nevertheless, two SRH defects with different slopes can be identified from the injection dependent lifetime.

III. DETERMINATION OF THE DEFECT FINGERPRINT ξ

On the Cz-Si wafer, the area outside the low lifetime rings features charge carrier lifetimes in the order of several milliseconds and is mainly limited by surface and Auger recombination for all investigated temperatures and injection levels. To compute the SRH lifetime limitation due to the circular distributed defect, we can therefore correct for the effect of surface and Auger recombination using the lifetimes in the unaffected areas, assuming lateral homogeneity of these recombination channels. The measured lifetime of the NOC Si sample is corrected by Auger recombination according to the model of Richter *et al.*[19] We fit the resulting SRH lifetime for the different temperatures and determine the characteristic defect parameters ξ at every pixel which represents a fingerprint for impurities independent of the impurity concentration.[9]

The defect fingerprint ξ for n-type Si

$$\xi := \frac{\mathrm{d}\tau_{\mathrm{SRH}}}{\mathrm{d}Y} \Bigg/ \lim_{Y\to 1} \tau_{\mathrm{SRH}} = \frac{1}{Q+1} - \frac{1}{n_0}\left(\frac{Q \times n_1 + p_1}{Q+1}\right) \quad (1)$$

is fitted as in Ref. 9 from the injection dependent lifetime measurement τ_{SRH} for every temperature. n_1 and p_1 are the SRH densities and $Q = \sigma_e/\sigma_h$ (also denoted k in literature) is the ratio of the capture cross sections for electrons (σ_e) and holes (σ_h). A detailed derivation for Equation (1) can be found in Ref. 7 (be aware of a typing error in Equations (12) and (13) of Ref. 7). The equation of the defect fingerprint ξ and all other equations for the p-type case are given in the Appendix. In our analysis we assume that the lifetime at a specific temperature is dominated by two independent SRH defects. Despite this restriction of the fitting quality the analysis enables the detection of more than two defects as long

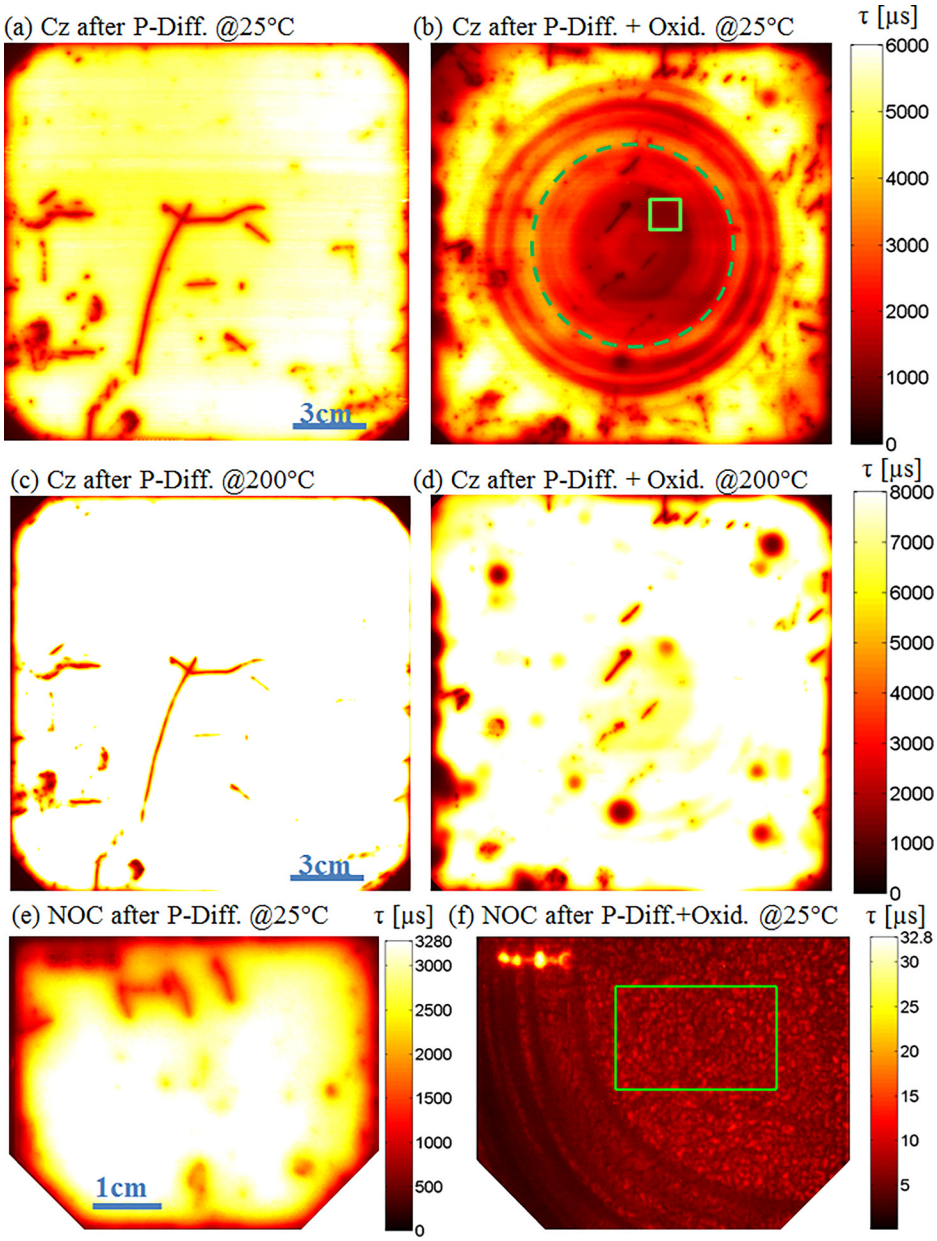

FIG. 1. Minority charge carrier lifetime images under illumination corresponding to ~1/100 sun equivalents. (a) Cz Si wafer subjected to phosphorus diffusion measured at 25 °C and (c) at 200 °C, (b) Cz Si wafer subjected to phosphorus diffusion and oxidation measured at 25 °C and (d) at 200 °C, (e) NOC Si wafer subjected to phosphorus diffusion, and (f) NOC Si wafer subjected to phosphorus diffusion and oxidation both measured at 25 °C.

as their critical temperatures,[6] i.e., the temperature at which the low injection recombination rate of the respective defect starts changing drastically, are well enough separated and the defects dominate the lifetime at different temperatures. If more than two defects are comparably dominant at a given temperature, the fitting can be altered, allowing more defects as discussed in Ref. 9.

In Figure 3 the resulting ξ maps for defect A and defect B of the analyzed samples can be found for various temperatures. Pixels in which the fit is not converging or the analysis could not be applied are grey in the figures. The ξ values decrease with increasing temperature as expected from theory.[9] However, below a critical temperature T^* the defect parameter ξ is almost constant, e.g., ξ_A in the NOC Si sample is constant below 75 °C. The ξ value close to 1 of defect A in the Cz Si sample is an indication that the critical temperature is close to 25 °C. In both samples the critical temperature for defect B could be equal to or smaller than 25 °C. Although measured lifetimes dominated by Auger recombination are not considered in the SRH fits, the procedure becomes less robust in areas with weak defect limitation and thus strong influences of surface or Auger recombination. This leads to the least unambiguous results in areas featuring highest lifetime, e.g., the results for Cz Si at 120 °C, a temperature at which the circular distributed defects are only slightly visible due to low recombination activity. For this reason, we concentrate on the inner part of the Cz Si wafer, i.e., the center region and the surrounding rings in the following analysis, marked with a green dotted circle in Figure 1(a).

Two regions with slightly different ξ for defect A can be distinguished in this area: the low lifetime center of the wafer and the surrounding ring area. In the low lifetime center of the Cz Si sample the ξ values of both defects decrease with every temperature step. Interestingly, we can even see that the ξ values at surface scratches differ significantly from the surrounding area. Although the rings are also visible in the ξ maps of the NOC Si sample, the maps are more homogeneous than the ξ maps of the Cz Si sample.

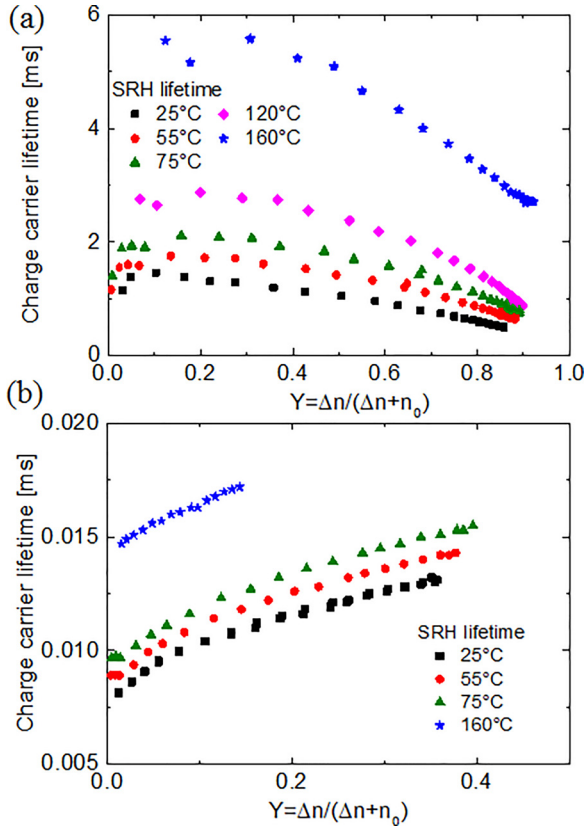

FIG. 2. Averaged injection dependent minority carrier lifetime for different temperatures in the Cz (a) and NOC (b) sample. The areas which are included in the average are marked with a green rectangle in Figures 1(b) and 1(d).

IV. DETERMINATION OF THE TRAP LEVELS

In the next step the evolution of ξ with temperature is analyzed to determine the energy level and the ratio of the capture cross sections. For every pixel we determine the lowest temperature T with $\Delta\xi(T) := \xi(298\,\mathrm{K}) - \xi(T) > \mathrm{C_{Threshold}}$. $\mathrm{C_{Threshold}}$ is an empirical parameter, which represents the sensitivity of the method on lifetime variations. We used 0.03 in the presented analyses. For very low $\mathrm{C_{Threshold}}$ measurement uncertainties might falsify the results, whereas for values >0.05 other recombination channels might influence the results and the accuracy of the analysis decreases. The value $\Delta\xi(T^*)$ with the lowest temperature is used for further calculations.

Given the case that $\xi(298\,\mathrm{K}) - \xi(298\,\mathrm{K} + \Delta T) < \mathrm{C_{Threshold}}$ the second term in Equation (1), i.e., n_1 and p_1, can be neglected for 298 K and we can estimate the ratio $Q = \sigma_e/\sigma_h$ of the capture cross sections for electrons (σ_e) and holes (σ_h) for n-type Si with

$$Q(298\mathrm{K}) \approx \frac{1 - \xi(298\mathrm{K})}{\xi(298\mathrm{K})}. \tag{2}$$

The criterion is only fulfilled for the NOC defect A as the critical temperature in this case is larger than 298 K. For others, Equation (2) determines an upper limit of Q (lower limit for p-type). For negative $\xi(298\,\mathrm{K})$ due to a dominant n_1 or p_1 term, e.g., Cz defect B, Equation (2) cannot be applied at all. However, even the upper (p-type Si: lower) limit can be very helpful for the identification of defects. For the Cz defect A, Q is smaller than 0.1 and in the rings outside the

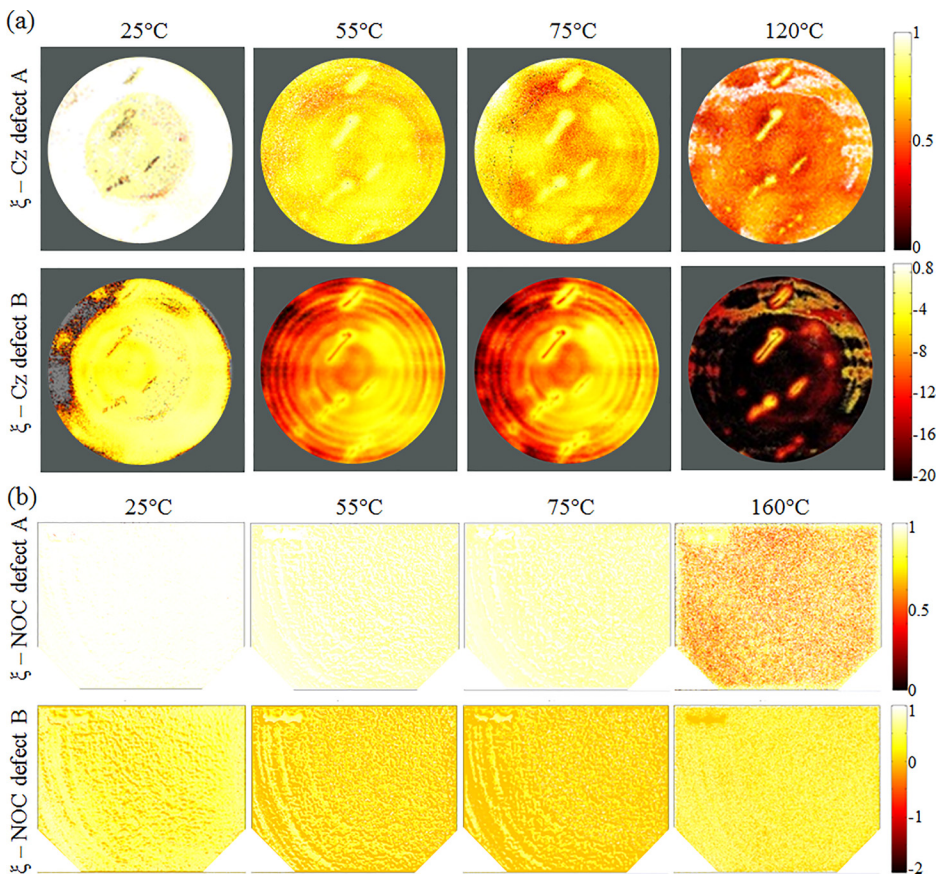

FIG. 3. ξ maps for SRH defects A and B obtained for Cz (a) and NOC (b) samples at different temperatures giving a fingerprint of the defects. For Cz samples the area outside the circular distributed defects is not considered in the analysis and is marked in grey. Other grey pixels indicate that either the fit or the analysis was not successful, e.g., because of a dominance of Auger recombination.

center even ≤ 0.001 (Fig. 4). Thus, we can conclude that the defect which we named Cz defect A is not the same as the SRH defect 1 of oxide precipitates with $Q = 157$ as identified by Murphy *et al.*[7,17] but might be the SRH defect 2 of oxide precipitates with $Q = 1/1200$. For the NOC sample we get a mean $Q_{\text{Defect A}} = 0.01$ which is in the same range as the Cz defect and a mean $Q_{\text{Defect B}} \leq 14$. As a next step the trap levels are compared with the literature values.

A strong decrease of ξ with increasing temperature, i.e., $\Delta\xi(T) > C_{\text{Threshold}}$, can be caused either by the SRH density n_1 or p_1. If we neglect a possible temperature dependence of the capture cross sections and thus Q, we can calculate n_1 in n-type silicon with

$$n_1 = \frac{\Delta\xi(T^*)}{1 - \xi(298\text{K})} \times n_0 \quad \text{for } n_1 \gg p_1 \tag{3}$$

and

$$p_1 = \frac{\Delta\xi(T^*)}{\xi(298\text{K})} \times n_0 \quad \text{for } p_1 \gg n_1. \tag{4}$$

Finally we can calculate the trap level E_t with

$$E_C - E_t = -\ln\left(\frac{n_1}{N_C(T^*)}\right) \times k_B T^* \quad \text{for } n_1 \gg p_1 \tag{5}$$

or

$$E_t - E_V = -\ln\left(\frac{p_1}{N_V(T^*)}\right) \times k_B T^* \quad \text{for } p_1 \gg n_1, \tag{6}$$

where N_C and N_V are the density of states at the conduction and valence band edge, respectively. For $\xi(298\,\text{K}) - \xi(T_2) > C_{\text{Threshold}}$, i.e., if the trap level of the defect is quite shallow, we calculate only a highest possible distance of the energy level E_t from E_C or E_V for every temperature T with (n-type Si)

$$E_C - E_t \leq -\ln\left(\frac{-\xi(T) \times n_0}{N_C(T)}\right) \times k_B T \quad \text{for } n_1 \gg p_1 \tag{7}$$

or

$$E_t - E_V \leq -\ln\left(\frac{-\xi(T) \times n_0}{N_V(T)}\right) \times k_B T \quad \text{for } p_1 \gg n_1 \tag{8}$$

and assume the most shallow level for the images. In principle the energy level E_t as well as capture cross section ratio Q can also be determined from the temperature dependence of ξ.[8] However, an exponential fit of ξ values determined at only few temperatures is error-prone and thus additional temperature dependent measurements on a wide temperature range would be necessary.

The trap levels of the defects in the Cz and the NOC samples are shown in Figure 5. From the capture cross section ratios we conclude that defect A in both the NOC and Cz sample could be the SRH defect 2 for oxide precipitates found by Murphy *et al.*[7] which is in the lower band half. With the same argument defect B is assumed to be defect 1 of oxide precipitates, located in the upper band half. Thus, we can focus on the images marked with a green rectangle in Figure 5. For defect A in the Cz sample we get $E_C - E_t = 0.18$ eV in the center and a shallower trap level ($E_C - E_t \sim 0.07$ eV) in the rings outside the center. For defect B in the Cz sample we can only extract an upper limit of the trap level $E_t - E_V \leq 0.24$ eV.

The defect parameters found in the Cz samples agree well with the SRH defects associated with oxide precipitates. Especially the (arithmetic) averaged values in the ring structure surrounding the center of the Cz sample (defect A: $E_C - E_t \sim 0.07$ eV and $Q_A \leq 0.001$; defect B: $E_t - E_V \leq 0.24$ eV) are in very good agreement with $E_C - E_t = 0.08$ eV having $Q = 1/1200$ and $E_t - E_V = 0.22$ eV having $Q = 157$ found by Murphy *et al.*[7] In the center of the Cz wafer the trap level of

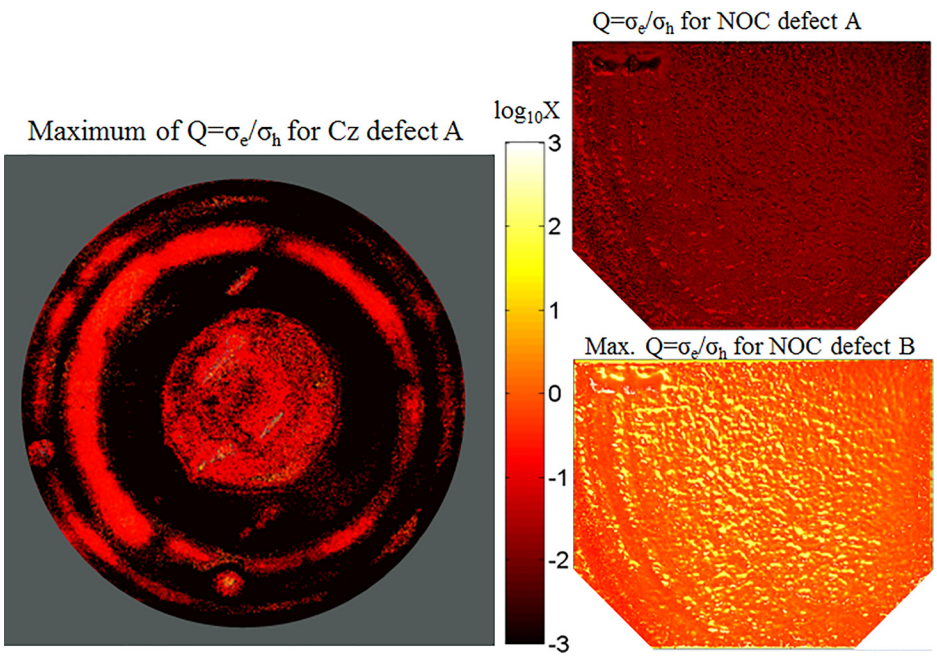

FIG. 4. Ratio of the capture cross sections $Q = \sigma_e/\sigma_h$ for the Cz defect A and the NOC defects. The Cz defect A and the NOC defect B give only maximum values. The ξ of the Cz defect B is already negative at room temperature which impedes the calculation of a Q value with Equation (2).

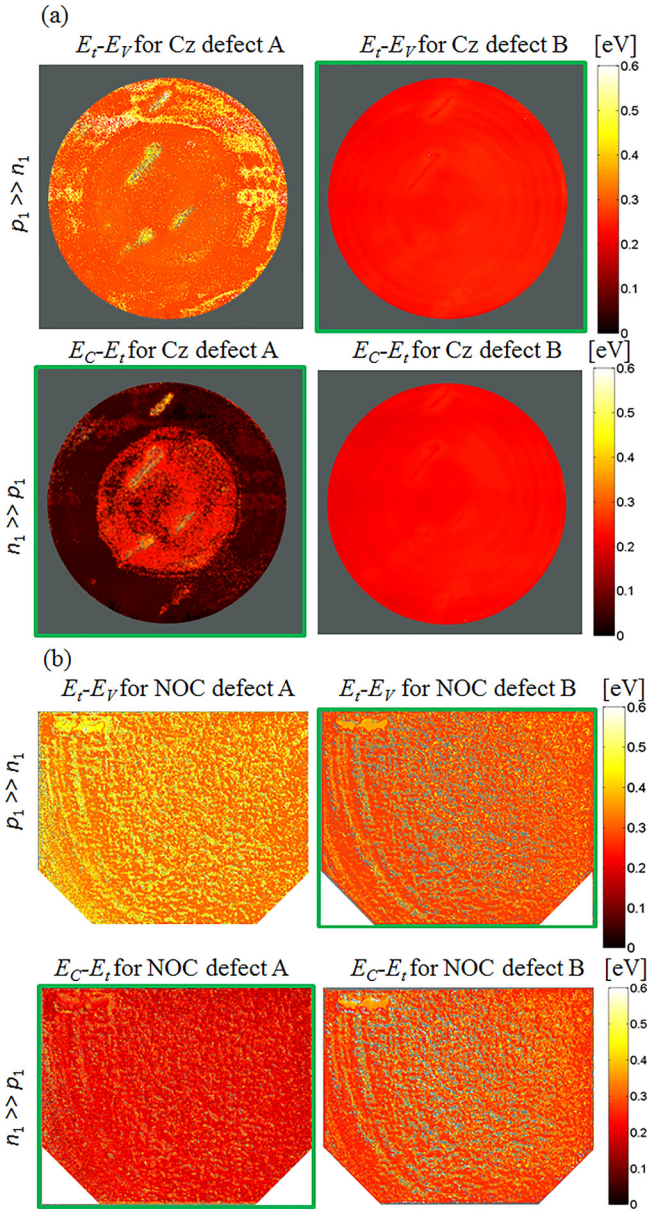

FIG. 5. Trap levels of the defects in the Cz and the NOC sample for the two possible cases, $n_1 \gg p_1$ and $p_1 \gg n_1$. If we assume that the defects are related to oxide precipitates, we can concentrate on the images marked with a green rectangle from the Q analysis. The images for defect B show the maximum energy levels. Grey areas indicate pixels at which either the fit or the analysis was not successful, e.g., because of a domination of Auger recombination.

defect A seems to be slightly deeper. The SRH parameters found by Murphy *et al.*[7] were extracted from quasi-steady-state photoconductance (QSSPC) measurements. Thus slight deviations from our spatially resolved analysis are expected due to the averaging over a large area of the QSSPC method.[18] It is worth noticing that in Ref. 7 a slightly increasing lifetime with injection density was measured at low injection in a n-type sample too (e.g., Fig. 2(a) in Ref. 7), which is a hint for a slightly deeper trap level. In our analysis the temperature dependence of the capture cross sections found for both defects in Ref. 7 is neglected. We estimated a slightly shallower defect A and a slightly deeper defect B if we assume the temperature dependency found in Ref. 7. With the temperature dependence $\Delta\xi$ for defect A could be $\sim$0.003 higher and $\sim$0.005 lower for defect B in Equations (3) and (4), which is small compared with other uncertainties.

For the defects in NOC silicon we found a mean value of $E_C - E_t = 0.22$ eV for defect A and $E_t - E_V \leq 0.31$ eV for defect B. Both trap levels differ significantly from the ones of the Cz defects (especially outside the Cz center) and the oxide precipitates studied by Murphy *et al.*[7] This reflects the missing decreasing slope in the injection dependent SRH lifetimes curves of the NOC sample.

V. CONCLUSIONS

The technique of temperature- and injection-dependent photoluminescence imaging is extended to high temperature PL measurements of up to 200 °C to be able to carefully study even deep defects in silicon. The technique allows us to determine the trap levels and the ratio of the capture cross sections of different defects in one sample and thus enables identification of these lifetime limiting defects. We studied the circular distributed defects causing inhomogeneity in lifetime across the wafer area and resulting in performance loss in both n-type Cz and NOC wafers. The differences between the defect parameters found in the Cz samples ($\leq$0.24 eV above the valence band and depending on the wafer position 0.04–0.2 eV below the conduction band) and literature values for homogeneously generated oxide precipitates[7] are within the uncertainty range of the method. This strongly supports the assumption that the defects in the low lifetime rings of the investigated Cz are decorated oxide precipitates similar to those in Refs. 7 and 12. In contrast the trap levels found in the NOC sample ($\leq$0.31 eV above the valence and 0.22 eV below the conduction band) differ significantly from the values for Cz and the ones found in Refs. 7 and 12, although the formation of the defect and the ring like structure are strong indications for oxide precipitates, too. The significantly different defect levels could be explained by a different morphology and/or impurity decoration of the oxide precipitates. If this hypothesis is true then the idea of Murphy *et al.*[7,12] that all oxide precipitates in Cz silicon can be described with the same defect parameters is not viable for silicon fabricated by other methods.

ACKNOWLEDGMENTS

The authors thank Rebekka Eberle and Georg Diez for helping with calibration measurements. Funding for this work was partly provided by the National Science Foundation (NSF) and the Department of Energy (DOE) under NSF CA No. EEC-1041895. This work was partly funded by the German Federal Ministry for Economic Affairs and Energy within the research project "THESSO" under Contract No. 0325491 (THESSO). A. Youssef acknowledges MISTI Germany program for partly funding her stay as a visiting researcher at Fraunhofer ISE. M.A. Jensen acknowledges support by the National Science Foundation Graduate Research Fellowship under Grant No. 1122374.

APPENDIX: EQUATIONS FOR p-TYPE Si

For p-type Si Equations (1)–(4) are the following:

$$\xi := \frac{d\tau_{SRH}}{dX} \Big/ \lim_{X\to 1} \tau_{SRH} = \frac{Q}{Q+1} - \frac{1}{p_0}\left(\frac{Q\times n_1 + p_1}{Q+1}\right). \quad \text{(A1)}$$

With $X = \Delta n/(\Delta n + p_0)$ and the net doping concentration p_0

$$Q(298\text{K}) \approx \frac{\xi(298\text{K})}{1-\xi(298\text{K})}, \quad \text{(A2)}$$

$$n_1 = \frac{\Delta\xi(T^*)}{\xi(298\text{K})} \times p_0 \quad \text{for } n_1 \gg p_1, \quad \text{(A3)}$$

and

$$p_1 = \frac{\Delta\xi(T^*)}{1-\xi(298\text{K})} \times p_0 \quad \text{for } p_1 \gg n_1. \quad \text{(A4)}$$

Equations (5) and (6) are similar in n- and p-type Si. In the case of a shallow defect in p-type Si, i.e., $\xi(298\,\text{K}) - \xi(T_2) > \text{C}_{\text{Threshold}}$ and $n_1 \gg p_1$ we can determine the highest possible distance of the energy level E_t from the conduction band E_C from the minimum of

$$E_C - E_t \le -\ln\left(\frac{-\xi(T)\times p_0}{N_C(T)}\right) \times k_B T \quad \text{(A5)}$$

calculated at every temperature T. For $p_1 \gg n_1$ the maximum distance from the valence band (E_V) is determined from

$$E_t - E_V \le -\ln\left(\frac{-\xi(T)\times p_0}{N_V(T)}\right) \times k_B T. \quad \text{(A6)}$$

[1] M. C. Schubert, H. Habenicht, and W. Warta, IEEE J. Photovoltaics **1**, 168 (2011).
[2] H. Habenicht, M. C. Schubert, and W. Warta, J. Appl. Phys. **108**, 34909 (2010).
[3] D. Macdonald, J. Tan, and T. Trupke, J. Appl. Phys. **103**, 73710 (2008).
[4] S. Y. Lim, F. E. Rougieux, and D. Macdonald, Appl. Phys. Lett. **103**, 92105 (2013).
[5] K. Graff, *Metal Impurities in Silicon-Device Fabrication* (Springer, Berlin, 1999).
[6] S. Rein, T. Rehrl, W. Warta, and S. W. Glunz, J. Appl. Phys. **91**, 2059 (2002).
[7] J. D. Murphy, K. Bothe, R. Krain, V. V. Voronkov, and R. J. Falster, J. Appl. Phys. **111**, 113709 (2012).
[8] S. Rein, *Lifetime Spectroscopy: A Method of Defect Characterization in Silicon for Photovoltaic Applications* (Springer-Verlag, Berlin, 2005).
[9] L. E. Mundt, M. C. Schubert, J. Schön, B. Michl, T. Niewelt, F. Schindler, and W. Warta, IEEE J. Photovoltaics **5**, 1503 (2015).
[10] J. Haunschild, I. Reis, J. Geilker, and S. Rein, Phys. Status Solidi RRL **5**, 199 (2011).
[11] R. Falster and V. Voronkov, Mater. Sci. Forum **2008**, 45.
[12] J. D. Murphy, R. E. McGuire, K. Bothe, V. V. Voronkov, and R. J. Falster, Sol. Energy Mater. Sol. Cells **120**, 402 (2014).
[13] R. Falster, V. Voronkov, and F. Quast, Phys. Status Solidi B **222**, 219 (2000).
[14] K. Nakajima, S. Ono, R. Murai, and Y. Kaneko, J. Electron. Mater. **45**, 2837 (2016).
[15] M. Kivambe, D. M. Powell, S. Castellanos, M. A. Jensen, A. E. Morishige, K. Nakajima, K. Morishita, R. Murai, and T. Buonassisi, J. Cryst. Growth **407**, 31 (2014).
[16] K. Nakajima, R. Murai, S. Ono, K. Morishita, M. Kivambe, D. M. Powell, and T. Buonassisi, Jpn. J. Appl. Phys., Part 1 **54**, 15504 (2015).
[17] J. D. Murphy, M. Al-Amin, K. Bothe, M. Olmo, V. V. Voronkov, and R. Falster, J. Appl. Phys. **118**, 215706 (2015).
[18] J. A. Giesecke, M. C. Schubert, B. Michl, F. Schindler, and W. Warta, Sol. Energy Mater. Sol. Cells **95**, 1011 (2011).
[19] A. Richter, S. W. Glunz, F. Werner, J. Schmidt, and A. Cuevas, Phys. Rev. B **86**, 165202 (2012).